

# EAVL: Explicitly Align Vision and Language for Referring Image Segmentation

Yichen Yan<sup>1</sup>, Xingjian He<sup>1</sup>, Wenxuan Wang<sup>1</sup>, Sihan Chen<sup>1,2</sup>, Jing Liu<sup>1,2\*</sup>

<sup>1</sup>Institute of Automation, Chinese Academy of Sciences

<sup>2</sup>School of Artificial Intelligence, University of Chinese Academy of Sciences

yanyichen2021@ia.ac.cn, xingjian.he@nlpr.ia.ac.cn, wangwenxuan2023@ia.ac.cn, sihan.chen@nlpr.ia.ac.cn, jliu@nlpr.ia.ac.cn

## Abstract

Referring image segmentation aims to segment an object mentioned in natural language from an image. The main challenge is text-to-pixel fine-grained correlation. Previous approaches mainly focus on the fusion of vision and language features and fused features are directly fed into a decoder and pass through convolutions with a fixed kernel to obtain the result, which follows a similar pattern as traditional image segmentation. These methods do not explicitly align language and vision features in the segmentation stage, resulting in a suboptimal text-to-pixel fine-grained correlation. In this paper, we propose a network that explicitly aligns vision and language features named EAVL. Instead of using a fixed convolution kernel, we propose a Vision-Language Aligner which explicitly aligns the vision and language features in the segmentation stage by dynamic convolution kernels. In our method, a series of dynamic convolution kernels are generated based on the input language and image which are used to explicitly align the vision and language features. Specifically, we generate multiple queries that represent different emphases of the language expression. These queries are transformed into a series of query-based convolution kernels. Then, we utilize these kernels to do convolutions in the segmentation stage and obtain a series of segmentation masks. The final result is obtained through the aggregation of all masks. Our method can not only fuse vision and language features effectively but also exploit their potential in the segmentation stage. And most importantly, we explicitly align language features of different emphases with the image features to achieve text-to-pixel fine-grained correlation. Our method surpasses previous state-of-the-art methods on RefCOCO, RefCOCO+, and G-Ref by large margins.

## 1 Introduction

Referring image segmentation (Hu, Rohrbach, and Darrell 2016; Liu et al. 2017; Li et al. 2018), which aims to segment an object referred by natural language expression from an image, is a fundamental vision-language task. This task has numerous potential applications, including interactive image editing and human-object interaction (Wang et al. 2019). Referring image segmentation poses a major challenge called text-to-pixel fine-grained correlation. Text-to-

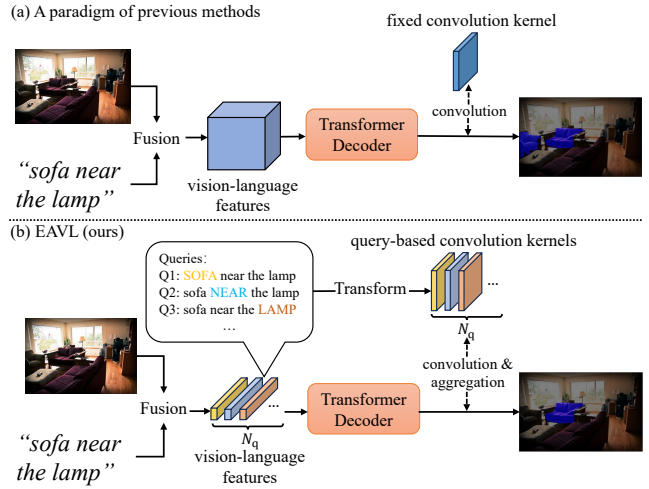


Figure 1: (a) In the previous methods (i.e., VLT (Ding et al. 2021)), the vision-language features obtained after fusion are directly input into a Transformer Decoder, and the final result is obtained using a fixed convolution kernel. This approach is similar to the method employed in the segmentation stage of traditional image segmentation. (b) Our approach diverges from the previous methods by generating special vision-language features called queries and transforming them into a series of dynamic query-based convolution kernels. Our method not only maximizes the potential of vision-language features but also explicitly aligns the vision features with language features to achieve text-to-pixel fine-grained correlation.

pixel fine-grained correlation is to correlate vision and relevant language information at the pixel level.

Early works have primarily focused on how to fuse vision and language features effectively, with a common approach that utilizes concatenation and convolution to fuse them. With the widespread use of attention mechanism, several methods (Ding et al. 2021; Kim et al. 2022) have adopted vision-language attention mechanism to learn cross-modal features more effectively. Recently, some methods (Wang et al. 2022; Yang et al. 2022) have started using pre-trained models to align and fuse the features. Prior methods have primarily emphasized the enhancement of cross-modal fea-

\*Corresponding author

ture fusion. They use convolutions with a fixed kernel in the segmentation stage which implicitly aligns the vision and language features. However, addressing text-to-pixel fine-grained correlation requires explicitly aligning the vision features and language features. This explicit alignment ensures that the image and language are mutually influenced and contribute to accurate referring image segmentation.

As illustrated in Figure 1(a), previous methods extract visual features from images and textual features from language expressions separately. These features are then fused into vision-language features. However, in the subsequent stage, these methods follow a conventional approach by directly inputting the fused features into a transformer decoder and applying convolution operations with a learned fixed convolution kernel. This traditional approach has two drawbacks: (1). It only focuses on the fusion process of obtaining the vision-language features without fully harnessing their inherent potential in the segmentation stage. (2). No matter what language or image input, a fixed convolution kernel is used to get the final prediction mask, resulting in only an implicit alignment of vision and language features in the segmentation stage.

In this paper, we argue that the fused vision-language features have untapped potential to guide explicit alignment in the segmentation stage. In Figure 1(b), we introduce a method that uses a series of dynamic convolution kernels generated based on the input language and image. In order to accomplish this, we first extract vision and language features respectively, and fuse them into a series of queries. Each query represents a different emphasis of the input sentence. These queries, also denoted as vision-language features, are not only fed into a Transformer Decoder as usual but also transformed into a series of dynamic query-based convolution kernels. These multiple dynamic kernels are then used to do convolutions with the output of the Transformer Decoder, resulting in a series of corresponding segmentation masks. The final result is obtained by the aggregation of these masks. This method of generating different convolution kernels depending on the inputs enables explicit alignment of vision and language features in the segmentation stage. Our method maximizes the potential of vision-language features as well as explicitly aligns the vision features with language features of different emphasis. Moreover, this explicit alignment facilitates text-to-pixel fine-grained correlation and obtains accurate results by aggregating multiple masks obtained through query-based convolution kernels.

Specifically, we introduce a new structure for referring image segmentation that effectively utilizes the potential of vision-language features to explicitly align the vision and language features. As illustrated in Figure 2, We use CLIP (Radford et al. 2021) to extract language features and image features, then we generated multiple queries and each query represents a different emphasis of the input sentence. These queries are not only fed into a Transformer Decoder like the previous approach but also send to a Vision-Language Aligner which includes a Multi-Mask Generator and a Multi-Query Estimator. In Multi-Mask Generator, these queries are transformed into a series of query-based

convolution kernels to do convolution with the outputs of the Transformer Decoder. Therefore, each query will produce a mask representing a different emphasis of the language expression. These queries will be also used to generate a series of scores that represent the importance of themselves in Multi-Query Estimator. The final result is obtained by computing the weighted sum of all the masks. By this approach, we explicitly align language features of different emphases with the image features. Overall, our novel structure enhances the exploitation of these queries, moreover, these dynamic query-based convolution kernels achieve an explicit alignment of the vision and language features, resulting in an effective text-to-pixel fine-grained correlation and accurate results. In summary, our main contributions are listed as follows:

- We introduce the EAVL, a novel framework for referring image segmentation. Our approach employs a Vision-Language Aligner in the segmentation stage that explicitly aligns the vision and language features to effectively address the text-to-pixel fine-grained correlation.
- We generate a series of queries, which are also vision-language features. Instead of only sending them into a Transformer Decoder as usual, we transform them into query-based convolution kernels and produce corresponding masks to obtain the final results. By doing so, we not only obtain vision-language features but also effectively exploit their potential to enhance the overall performance of the model.
- The experimental results on three challenging benchmarks significantly outperform previous state-of-the-art methods by large margins.

## 2 Related Work

**Referring Image Segmentation.** Referring image segmentation aims at segmenting a specific region in an image by comprehending a given natural language expression (Hu, Rohrbach, and Darrell 2016). This task is fundamental and challenging, requiring a deep understanding of both vision and language. It has the potential to be applied in a wide range of domains, such as interactive image editing and human-object interaction. Early works (Li et al. 2018; Liu et al. 2017) first extracted vision and language features by CNN and LSTM respectively, and then directly concatenated vision and language features to obtain final segmentation results. Multi-task collaborative network (Luo et al. 2020b) achieves joint learning of referring expression comprehension and segmentation. As the attention mechanism and transformer arouse more and more interest, a series of works are proposed to adopt the attention mechanism to fuse the vision and language features. For example, VLT (Ding et al. 2021) employs a transformer to build a network with an encoder-decoder attention mechanism for enhancing the global context information LAVT (Yang et al. 2022) conducts multi-modal fusion at intermediate levels of the transformer-based network. However, most of the previous work focuses on how to improve cross-modal feature fusion effectively, without fully exploiting the potential of the fused vision-language features. Moreover, they use the

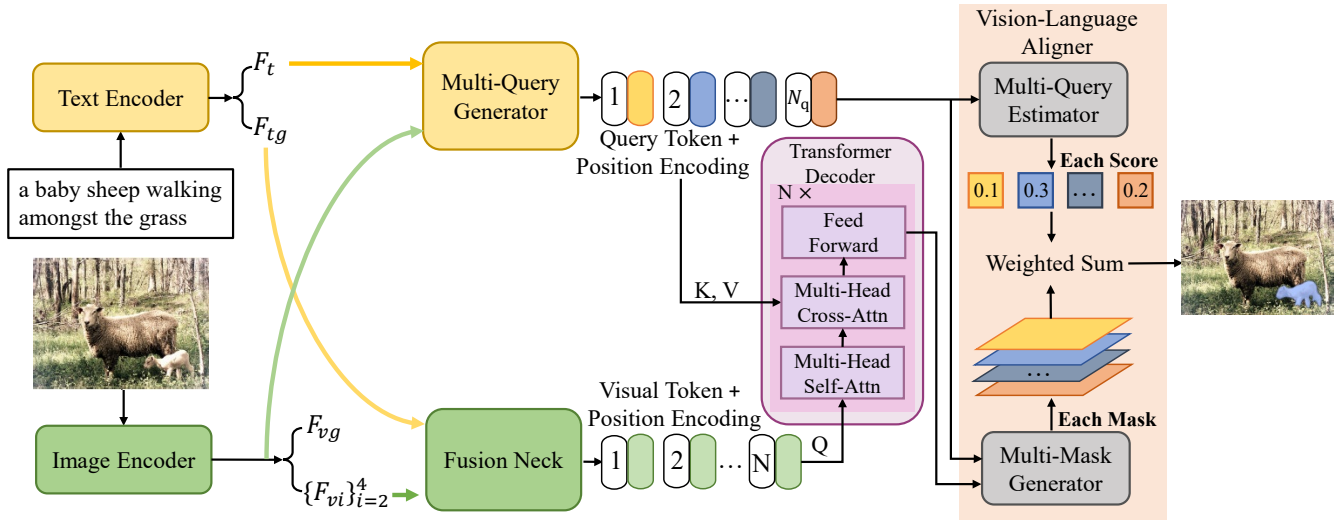


Figure 2: EAVL mainly consists of a text encoder, an image encoder, a Multi-Query Generator, a Transformer Decoder, and a Vision-Language Aligner. The Vision-Language Aligner has two parts, a Multi-Mask Generator and a Multi-Query Estimator.

fixed convolution kernel which only implicitly aligns the vision and language features, resulting in a suboptimal text-to-pixel fine-grained correlation.

**Vision-Language Pre-training.** Vision-Language Pre-training model is a type of deep learning model that aims to learn joint representations of both visual and textual information. These models have been shown to be effective in a wide range of natural language processing (NLP) and computer vision (CV) tasks. As a milestone, CLIP (Radford et al. 2021) employs a contrastive learning strategy on a huge amount of image-text pairs and shows impressive transferable ability over 30 classification datasets. Motivated by this work, CRIS (Wang et al. 2022) employs CLIP (Radford et al. 2021) pre-trained on 400M image text pairs and transformer decoder to transfer the CLIP’s knowledge from text-to-image matching to text-to-pixel matching. However, the approach only focuses on fine-grained visual representations and neglects the importance of global visual information, which is a critical aspect of CLIP. Because both global visual and textual information are used to calculate the contrastive score. More important, it only implicitly aligns the vision and language features by CLIP. Our approach, on the other hand, also employs CLIP to address referring image segmentation, but with a focus on both fine-grained and global visual information, and uses them explicitly to align the vision and language features.

### 3 Methodology

As illustrated in Figure 2, our proposed framework facilitates knowledge transfer to generate multiple queries and their corresponding masks to obtain the final prediction. Firstly, the framework takes an image and a language expression as input. We leverage ResNet (He et al. 2016)/ViT (Dosovitskiy et al. 2020) as the image encoder and a Transformer as the text encoder to extract image and text features, respectively. These extracted features are then combined in

the Fusion Neck to obtain the simple vision-language features. After that, we utilize the vision feature and the language features to generate multiple queries in Multi-Query Generator.

Then, the generated queries and simple vision-language features are input into the Transformer Decoder. The output of the decoder, along with the generated queries, are fed into the Multi-Mask Generator to produce multiple masks. Meanwhile, the Multi-Query Estimator uses the queries to determine the weights of each mask. Finally, we use those masks and their corresponding weights to calculate the weighted sum to obtain the final result.

#### 3.1 Image and Text Feature Extraction

**Text Encoder.** For a given language expression  $T \in \mathbb{R}^L$ , we utilize a Transformer to obtain text features  $F_t \in \mathbb{R}^{L \times C}$ . We follow CLIP (Radford et al. 2021), specifically, we prepend the text sequence with the [SOS] token and append it with the [EOS] token, denoting the beginning and end of the sequence, respectively. Additionally, we use the highest layer’s activations of the Transformer at the [EOS] token as the global feature for the entire language expression. This feature is linearly transformed and denoted as  $F_{tg} \in \mathbb{R}^{C'}$ . Here,  $C$  and  $C'$  represent the feature dimension, while  $L$  is the length of the language expression.

**Image Encoder.** For a given image  $I \in \mathbb{R}^{H \times W \times 3}$ , we extract not only local but also global visual representations. As an example, we use the ResNet encoder. In the architecture of CLIP image encoder, they take the ResNet encoder, there are 4 stages in total and we denote the feature as  $\{\mathbf{x}_i\}_{i=1}^4$ . Unlike the original ResNet, CLIP adds an attention pooling layer. Specifically, CLIP applies global average pooling to  $\mathbf{x}_4 \in \mathbb{R}^{H_4 \times W_4 \times C}$  to obtain a global feature, denoted as  $\bar{\mathbf{x}}_4 \in \mathbb{R}^C$ . Here,  $H_4$ ,  $W_4$ , and  $C$  are the height, width, and number of channels of  $\mathbf{x}_4$ . Then, CLIP concatenates the features  $[\bar{\mathbf{x}}_4, \mathbf{x}_4]$  and feeds them into a multi-head self-attention

layer.

$$[\bar{\mathbf{z}}, \mathbf{z}] = MHS A([\bar{\mathbf{x}}_4, \mathbf{x}_4]). \quad (1)$$

In CLIP, the final output of the image encoder is the global vision feature  $\bar{\mathbf{z}}$ , which is used to calculate the contrastive score with the global language feature from the Text Encoder. Other outputs  $\mathbf{z}$ , are typically disregarded. In contrast, CRIS (Wang et al. 2022) utilizes the other output  $\mathbf{z}$  as a feature map due to its adequate spatial information, while the global vision feature  $\bar{\mathbf{z}}$  is discarded.

In our proposed model, we leverage the multi-scale vision features  $\mathbf{x}_2 \in \mathbb{R}^{H_2 \times W_2 \times C}$  and  $\mathbf{x}_3 \in \mathbb{R}^{H_3 \times W_3 \times C}$  from the second and third stages of the ResNet, respectively. We transform them into  $F_{v2} \in \mathbb{R}^{H_2 \times W_2 \times C_2}$  and  $F_{v3} \in \mathbb{R}^{H_3 \times W_3 \times C_3}$  by two learnable matrices, respectively. In the fourth stage, we are different from both CLIP and CRIS, We not only use the vision feature  $\mathbf{z}$  for its sufficient spatial information but also incorporate the global vision feature  $\bar{\mathbf{z}}$  to capture the global information of the image. To accomplish this, we employ two learnable projection matrices to transform  $\mathbf{z}$  and  $\bar{\mathbf{z}}$  into  $F_{v4} \in \mathbb{R}^{H_4 \times W_4 \times C_4}$  and  $F_{vg} \in \mathbb{R}^{C_4}$ . It is also noted that for ViT (Dosovitskiy et al. 2020) backbone, vision features  $\mathbf{z}$  can be obtained similarly by excluding the class token of outputs, and global vision features  $\bar{\mathbf{z}}$  is the vector corresponding to the class token position in the output.

**Fusion Neck.** In the Fusion Neck, we perform a simple fusion of vision and language features, including  $F_{v2}$ ,  $F_{v3}$ ,  $F_{v4}$ , and the global language feature  $F_{tg}$ , to generate a vision feature that incorporates global language information. Initially, we fuse  $F_{v4}$  and  $F_{tg}$  to obtain  $F_{m4} \in \mathbb{R}^{H_3 \times W_3 \times C}$  using the following equation:

$$F_{m4} = Up(\sigma(F_{v4}W_{v4}) \cdot \sigma(F_{tg}W_{tg})), \quad (2)$$

In this process,  $Up(\cdot)$  denotes  $2 \times$  upsampling function, and  $\cdot$  denotes element-wise multiplication. We first transform the visual and textual representations into the same feature dimension using two learnable matrices,  $W_{v4}$  and  $W_{tg}$ , and then We apply ReLU activation function which is denoted as  $\sigma$  to generate  $F_{m4}$ . Subsequently, we obtain the multi-modal features  $F_{m3}$  and  $F_{m2}$  using the following procedures:

$$\begin{aligned} F_{m3} &= [\sigma(F_{m4}W_{m4}), \sigma(F_{v3}W_{v3})], \\ F_{m2} &= [\sigma(F_{m3}W_{m3}), \sigma(F'_{v2}W_{v2})], \\ F'_{v2} &= Avg(F_{v2}), \end{aligned} \quad (3)$$

Where  $Avg(\cdot)$  denotes a kernel size of  $2 \times 2$  average pooling operation with 2 strides,  $[\cdot, \cdot]$  denotes the concatenation operation. Subsequently, we concatenate the three multi-modal features ( $F_{m4}$ ,  $F_{m3}$ ,  $F_{m2}$ ) and use a  $1 \times 1$  convolution layer to aggregate them:

$$F_m = Conv([F_{m2}, F_{m3}, F_{m4}]), \quad (4)$$

Where  $F_m \in \mathbb{R}^{H_3 \times W_3 \times C}$ . Then, we use the 2D spatial coordinate feature  $F_{coord} \in \mathbb{R}^{H_3 \times W_3 \times 2}$  and concatenate it with  $F_m$  and flatten the result to obtain the fused vision features with global textual information which is denoted as  $F_{vt} \in \mathbb{R}^{H_3 \times W_3 \times C}$ .

$$\begin{aligned} F_{inte} &= Conv([F_m, F_{coord}]), \\ F_{vt} &= Flatten(F_{inte}). \end{aligned} \quad (5)$$

Here,  $Flatten(\cdot)$  denotes flatten operation and  $F_{inte} \in \mathbb{R}^{H_3 \times W_3 \times C}$  is intermediate features. After the flatten we obtain the  $F_{vt} \in \mathbb{R}^{N \times C}$ ,  $N = H_3 \times W_3 = \frac{H}{16} \times \frac{W}{16}$ , which will be utilized in the following process. As for ViT (Dosovitskiy et al. 2020) backbone, we directly extract its class token of outputs as a global vision feature and then use three convolutions on the other outputs to obtain the three features which have the same dimension as  $F_{v2}$ ,  $F_{v3}$  and  $F_{v4}$ . After that, the operations are the same as ResNet.

### 3.2 Multi-Query Generator

We use attention mechanism to generate new queries. Each query represents a different emphasis and will be transformed into a series of query-based convolution kernels in the Multi-Mask Generator.

As shown in Figure 2, the Multi-Query Generator takes multi-scale visual features  $\{F_{vi}\}_{i=2}^4$ , the global vision feature  $F_{vg}$ , and language features  $F_t$  as input and outputs a series of queries. To generate multiple queries, we first need to obtain dense vision features and fused language features.

**Dense Vision Features.** In according to obtain the dense vision features, we use the multi-scale vision features  $\{F_{vi}\}_{i=2}^4$ . The operations we take are very similar to those in Fusion Neck, the only difference is in Eq 2. We directly up-sample  $F_{v4}$  without element-wise multiplication by global language feature  $F_{tg}$  to obtain the  $F'_{m4}$ .

$$F'_{m4} = Up(\sigma(F_{v4}W_{v4})), \quad (6)$$

The rest operations are the same as the previous equations. After obtaining the intermediate features  $F'_{inte} \in \mathbb{R}^{H_3 \times W_3 \times C}$  just like  $F_{inte}$ , we apply three convolution layers to reduce the feature channel dimension size to the number of queries  $N_q$ . As a result, we obtain  $N_q$  feature maps, which are subsequently flattened in the spatial domain. Specifically, each feature map is flattened to a one-dimensional vector of length  $H_3 \times W_3$ , where  $H_3$  and  $W_3$  are the height and width of the dense vision feature maps, respectively. This results in  $F_{vd}$  of size  $N_q \times H_3 W_3$ , which contains detailed visual information. And the above process is formulated as follows,

$$F_{vd} = Flatten(Conv(F'_{inte}))^T, \quad (7)$$

**Fused language features.** Our approach incorporates both detailed vision features and holistic global vision features to guide the query generation process. We fuse the language features and the global vision feature by the following equation:

$$F_{tv} = \sigma(F_t W_t) \cdot \sigma(F_{vg} W_{vg}), \quad (8)$$

Here,  $F_{tv} \in \mathbb{R}^{L \times C}$ ,  $W_t$  and  $W_{vg}$  are two learnable matrices.

**Multi-Query Generation.** For referring image segmentation, the importance of different words in the same language expression is obviously different. In our approach, we use the dense vision features and the fused textual features to generate multiple queries, each corresponding to a different interpretation of the image. We do this by vision-guided attention and computing attention weights between

the dense vision features and the fused language features for each query.

In order to derive attention weights for fused textual features  $F_{tv}$ , we incorporate the dense vision features  $F_{vd}$ . We begin by applying linear projection to  $F_{vd}$  and  $F_{tv}$ . Then, for the  $n$ -th query ( $n = 1, 2, \dots, N_q$ ), we use the  $n$ -th dense vision feature vector  $f_{vdn} \in \mathbb{R}^{1 \times (H_3 W_3)}$ , along with the fused language features. Specifically, we use  $f_{tvi} \in \mathbb{R}^{1 \times C}$  to denote the feature of the  $i$ -th word ( $i = 1, 2, \dots, L$ ). The attention weight for the  $i$ -th word with respect to the  $n$ -th query is computed as the product of projected  $f_{vdn}$  and  $f_{tvi}$ :

$$a_{ni} = \sigma(f_{vdn} W_{vd}) \sigma(f_{tvi} W_a)^T, \quad (9)$$

In the equation,  $a_{ni}$  represents a scalar that indicates the importance of the  $i$ -th word in the  $n$ -th query, where  $W_{vd}$  and  $W_a$  are learnable matrices. To normalize the attention weights across all words for each query, we apply the Softmax function. The resulting values of  $a_{ni}$ , after being processed by Softmax, comprise the attention map  $A \in \mathbb{R}^{N_q \times L}$ . For the  $n$ -th query, we extract  $A_n \in \mathbb{R}^{1 \times L}$  ( $n = 1, 2, \dots, N_q$ ) from  $A$ , which represents the basis of the words on the  $n$ -th query. And  $A_n$  are used to generate the new queries as the following equation:

$$F_{qn} = A_n \sigma(F_{tv} W_{tv}). \quad (10)$$

The matrix  $W_{tv}$  is a learnable parameter, and  $F_{qn} \in \mathbb{R}^{1 \times C}$  is a new query. The set of all queries comprises the new matrix  $F_q \in \mathbb{R}^{N_q \times C}$ , which is also vision-language features predominantly influenced by language information. Then the  $F_q$  and fused vision features  $F_{vt}$  are fed into a standard transformer decoder to obtain fine-grained vision-language features  $F_s \in \mathbb{R}^{H_3 \times W_3 \times C}$ . In the transformer, Q is from  $F_{vt}$  and K, V are from  $F_q$ .

### 3.3 Vision-Language Aligner

In contrast to previous methods (Ding et al. 2021; Yang et al. 2022), which directly use a fixed learned convolution kernel to obtain the result, we leverage the queries and transform them into query-based convolution kernels. Therefore, the kernels are related to the specific language and image input. Specifically, we transform each query into a convolution kernel and use this query-based kernel to do convolution, resulting in a total of  $N_q$  masks. This process is conducted by the Multi-Mask Generator, and each mask represents a specific comprehension of the input language expression. Meanwhile, it is desirable to adaptively decide the importance of each mask, allowing the network to focus on the more important and more suitable ones. Specifically, we feed each query into the Multi-Query Estimator, which evaluates its importance and assigns a score reflecting the quality of the mask generated by this query-based kernel. We then use these scores to weigh and sum all the masks, resulting in the final mask.

**Multi-Mask Generator.** As illustrated in Figure 2, Multi-Mask Generator takes  $F_s$  and query vectors  $F_q$  as input. We extract one query  $F_{qn}$  from  $F_q$ , and  $F_{qn}$  is used to generate a query-based kernel. We use a dynamic convolution operation (Chen et al. 2020), and the parameters of the

query-based kernel come from  $F_{qn}$ . The detailed operations are as follows:

$$\begin{aligned} F_p &= Up(Conv(Up(F_s))), \\ F_{pn} &= \sigma(W_p F_{qn}), \end{aligned} \quad (11)$$

Here, we use  $2 \times$  upsampling and convolution operation to transform  $F_s$  into  $F_p \in \mathbb{R}^{4H_3 \times 4W_3 \times C_p}$ ,  $C_p = \frac{C}{2}$ . Then we use a linear layer to transform  $F_{qn}$  into  $F_{pn} \in \mathbb{R}^{9C_p+1}$ . For the vector  $F_{pn}$ , we take the first  $9C_p$  values as parameters of the  $3 \times 3$  convolution kernel whose number of channel is  $C_p$ , and we take the last value of  $F_{pn}$  as bias, resulting in a query-based convolution kernel  $W_{qn}$ , and then we utilize  $W_{qn}$  to do convolution with  $F_s$  obtain a mask, which is denoted as  $mask_n \in \mathbb{R}^{4H_3 \times 4W_3 \times 1}$ .

$$mask_n = \Psi_n(F_s, W_{qn}) \quad (12)$$

Here,  $\Psi_n$  denotes the  $3 \times 3$  convolution with the query-based convolution kernel  $W_{qn}$ .

**Multi-Query Estimator.** As illustrated in Figure 2, the Multi-Query Estimator takes the query vectors  $F_q$  as input and outputs  $N_q$  scores. Each score shows how much the query  $F_{qn}$  fits the context of its prediction, and reflects the importance of its response  $mask_n$  generated by itself. The Multi-Query Estimator first applies a multi-head self-attention layer and then employs a linear layer to obtain  $N_q$  scalar:

$$S_q = Softmax(W_s(MHSA(F_q))), \quad (13)$$

Here,  $S_q \in \mathbb{R}^{N_q \times 1}$ . The linear layer uses Softmax as an activation function to control the output range.

The final prediction is derived from the weighted sum of the mask obtained by the Multi-Mask Generator and the score obtained by the Multi-Query Estimator:

$$y = \sum_{n=1}^{N_q} S_{qn} mask_n. \quad (14)$$

Here,  $S_{qn}$  is  $n$ -th scalar of the  $S_q$ ,  $y$  denotes the final prediction mask. The model is optimized with cross-entropy loss.

## 4 Experiments

### 4.1 Implementation Details

**Experiment Settings.** Following previous works (Wang et al. 2022; Ding et al. 2021), we use ResNet-101 (He et al. 2016) and ViT (Dosovitskiy et al. 2020) as the image encoder. Input images are resized to  $480 \times 480$ . Due to the extra [SOS] and [EOS] tokens and the input sentences are set with a maximum sentence length of 17 for RefCOCO and RefCOCO+, and 22 for G-Ref. Each Transformer block has 8 heads, and the hidden layer size in all heads is set to 512, and the feed-forward hidden dimension is set to 2048. We conduct training for 100 epochs, utilizing the Adam optimizer with a learning rate of  $1e-5$  and a polynomial decay (Chen et al. 2014). We train the model with a batch size of 64 on 8 RTX Titan with 24 GPU VRAM.

Table 1: **Comparisons with the state-of-the-art approaches on three benchmarks.** We report the results of our method with various visual backbones. “\*” denotes the post-processing of DenseCRF (Krähenbühl and Koltun 2011). “†” denotes the Swin Transformer (Liu et al. 2021) pre-trained on ImageNet-22K (Deng et al. 2009). “-” represents that the result is not provided. IoU is utilized as the metric.

Method	Backbone	RefCOCO			RefCOCO+			G-Ref	
		val	test A	test B	val	test A	test B	val	test
RRN* (Li et al. 2018)	ResNet-101	55.33	57.26	53.95	39.75	42.15	36.11	-	-
MAttNet (Yu et al. 2018)	ResNet-101	56.51	62.37	51.70	46.67	52.39	40.08	47.64	48.61
MCN (Luo et al. 2020b)	DarkNet-53	62.44	64.20	59.71	50.62	54.99	44.69	49.22	49.40
CGAN (Luo et al. 2020a)	DarkNet-53	64.86	68.04	62.07	51.03	55.51	44.06	51.01	51.69
EFNet (Feng et al. 2021)	ResNet-101	62.76	65.69	59.67	51.50	55.24	43.01	-	-
LTS (Jing et al. 2021)	DarkNet-53	65.43	67.76	63.08	54.21	58.32	48.02	54.40	54.25
VLT (Ding et al. 2021)	DarkNet-53	65.65	68.29	62.73	55.50	59.20	49.36	52.99	56.65
ReSTR (Kim et al. 2022)	ViT-B	67.22	69.30	64.45	55.78	60.44	48.27	54.48	-
SeqTR (Li and Sigal 2021)	ResNet-101	70.56	73.49	66.57	61.08	64.69	52.73	58.73	58.51
CRIS (Wang et al. 2022)	ResNet-101	70.47	73.18	66.10	62.27	68.08	53.68	59.87	60.36
LAVT† (Yang et al. 2022)	Swin-B	<u>72.73</u>	<u>75.82</u>	<u>68.79</u>	62.14	68.38	55.10	61.24	62.09
EAVL(Ours)	ResNet-101	70.65	73.81	66.62	63.42	68.26	54.71	60.93	61.24
EAVL(Ours)	ViT-B	71.74	74.38	67.24	<u>64.05</u>	<u>68.41</u>	<u>56.82</u>	<u>61.87</u>	<u>62.21</u>
EAVL(Ours)	ViT-L	<b>75.01</b>	<b>77.81</b>	<b>71.59</b>	<b>68.44</b>	<b>72.81</b>	<b>59.86</b>	<b>66.52</b>	<b>67.28</b>

**Metrics.** Following previous works (Wang et al. 2022; Ding et al. 2021), we adopt two metrics to verify the effectiveness: IoU and Precision@ $X$ . The IoU calculates intersection regions over union regions of the predicted segmentation mask and the ground truth. The Precision@ $X$  measures the percentage of test images with an IoU score higher than the threshold  $X \in \{0.5, 0.6, 0.7, 0.8, 0.9\}$ , which focuses on the location ability of the method.

## 4.2 Datasets

We conduct our method on three standard benchmark datasets, RefCOCO (Yu et al. 2016), RefCOCO+ (Yu et al. 2016), and G-Ref (Nagaraja, Morariu, and Davis 2016), which are widely used in referring image segmentation task. Images in the three datasets are collected from the MS COCO dataset (Lin et al. 2014) and annotated with natural language expressions. The RefCOCO dataset contains 142,209 referring language expressions describing 50,000 objects in 19,992 images, while the RefCOCO+ dataset contains 141,564 referring language expressions for 49,856 objects in 19,992 images. The main difference between RefCOCO and RefCOCO+ is that RefCOCO+ only contains appearance expressions, and does not include words that indicate location properties (such as left, top, front) in expressions. G-Ref is another prominent referring segmentation dataset that contains 104,560 referring language expressions for 54,822 objects across 26,711 images. The language usage in the G-Ref is more casual and complex, and the sentence length of G-Ref are also longer on average. Furthermore, the G-Ref dataset has two partitions: one created by UMD (Nagaraja, Morariu, and Davis 2016) and the other by Google (Mao et al. 2016). In our paper, we report results on the UMD partition.

Table 2: **Influence of Query Numbers.**

$N_q$	IoU	Pr@50	Pr@60	Pr@70	Pr@80	Pr@90
32	67.26	79.45	75.58	68.71	52.65	14.91
24	<b>68.14</b>	<b>80.51</b>	<b>76.89</b>	<b>70.22</b>	<b>52.99</b>	<b>15.46</b>
16	67.59	79.86	75.82	69.03	52.71	14.80
8	66.85	78.69	75.03	68.05	52.55	14.83
4	66.13	78.08	74.39	68.54	52.12	14.29
2	65.80	77.53	74.19	68.13	51.87	14.39
1	65.42	76.62	72.73	66.26	51.41	13.84

## 4.3 Comparison to State-of-the-Arts

In Table 1, we evaluate EAVL against the state-of-the-art referring image segmentation methods on the RefCOCO, RefCOCO+, and G-Ref datasets using the IoU metric. As the results shows, when taking ResNet-101 as visual backbone, our method outperforms all previous methods using the same backbone and is only worse than LAVT (Yang et al. 2022) which uses a much stronger backbone Swin-Base (Liu et al. 2021). Under the settings that utilizing ViT-Base as visual backbone, our proposed method outperforms other methods on RefCOCO+ and G-Ref datasets. On RefCOCO datasets, we get a comparable result with other methods. We also conduct additional experiments using ViT-Large. Compared with LAVT, our method achieves higher performance with absolute margins of 3.13%~4.17% of RefCOCO, respectively. Similarly, our method attains noticeable improvements over the previous state of the art on RefCOCO+ with wide margins of 6.48%~10.14%. On the G-Ref dataset, our method surpasses the second-best methods on the validation and test subsets from the UMD partition by absolute margins



of 8.36% and 8.62%.

It is noteworthy that our model performs better on RefCOCO+ and G-Ref. We think the main reason is that our approach is to generate a series of queries that represent different emphases of the language expression. The sentences in RefCOCO are shorter and the descriptions are simpler. Therefore, these multiple queries should contain lots of redundant information, which makes our method less advantageous. The results also demonstrate our method can understand challenging language expressions from different aspects and effectively deal with harder datasets.

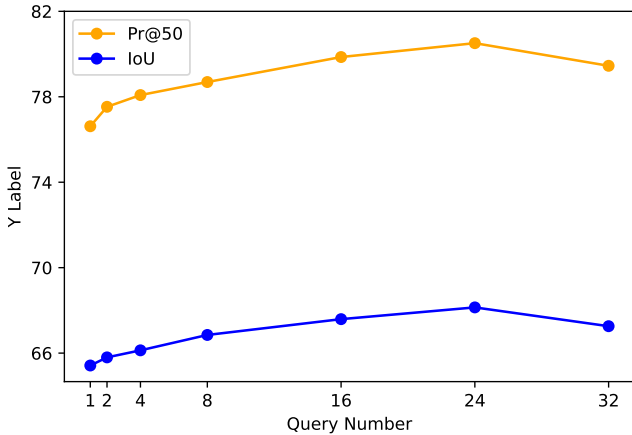


Figure 3: Performance gain by different query number  $N_q$

#### 4.4 Ablation Study

We conduct several ablations to evaluate the effectiveness of the key components in EAVL. We do the ablation study on the testA split of RefCOCO+, we use ResNet-50 as the vision backbone and the epoch is set to 50.

**Query number.** In order to clarify the influence of the query number  $N_q$ , we set the  $N_q$  to a series of different numbers. The results are reported in Table 2 and Figure 3. According to the result, multiple queries can improve the performance of our model which is about 4% from 1 query to 24 queries. However, larger  $N_q$  does not always bring a better result. With the increase of  $N_q$ , the performance will gradually level off or even decline. Eventually, We choose  $N_q = 24$  due to its best performance on all metrics

**Vision-Language Aligner.** The core of our method is using the Vision-Language Aligner. We employ dynamic query-based kernels to replace the fixed kernel. To demonstrate its effectiveness, we conduct a comparison experiment between the Vision-Language Aligner and convolution with a fixed kernel. In this experiment, we replaced the entire Vision-Language Aligner, including the Multi-Mask Generator and Multi-Query Estimator by convolutions with a fixed kernel. In this case, the input of the convolutions is only the output of the decoder without multiple queries. As shown in Table 3, the results show that under the setting of taking different values of  $N_q$ , Vision-Language Aligner consistently outperforms conventional fixed convolution kernels evidently. It is noted that both two methods generate multi-

Table 3: Comparison of convolutions with a fixed kernel (Fixed) and Vision-Language Aligner (Aligner) in the segmentation stage.

$N_q$	method	IoU	Pr@50	Pr@60	Pr@70	Pr@80	Pr@90
24	Aligner	<b>68.14</b>	<b>80.51</b>	<b>76.89</b>	<b>70.22</b>	<b>52.99</b>	<b>15.46</b>
	Fixed	66.75	78.39	74.54	68.39	52.08	15.08
16	Aligner	67.59	79.86	75.82	69.03	52.71	14.80
	Fixed	66.52	78.24	74.85	67.91	50.56	13.87
8	Aligner	66.85	78.69	75.03	68.05	52.55	14.83
	Fixed	66.09	77.38	73.89	67.05	49.60	13.41

Table 4: Ablation results of global vision feature  $F_{vg}$  and Multi-Query Estimator on the RefCOCO+ testA set. MQE denotes the Multi-Query Estimator.

$F_{vg}$	MQE	IoU	Pr@50	Pr@60	Pr@70	Pr@80	Pr@90
✓	✓	<b>68.14</b>	<b>80.51</b>	<b>76.89</b>	<b>70.22</b>	<b>52.99</b>	<b>15.46</b>
	✓	67.32	79.22	75.83	69.39	53.48	14.91
✓		66.69	78.54	75.35	69.03	52.43	14.73
		66.17	77.46	74.07	67.91	51.91	14.38

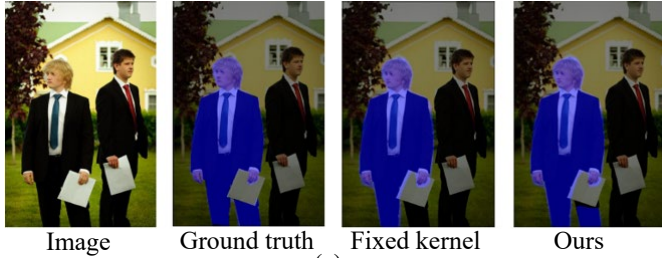
ple queries, but Vision-Language Aligner is more effective thanks to that it introduces explicit alignment of language and vision features during the segmentation stage, fully exploring the potential of multiple queries, and thus leading to more accurate text-to-pixel fine-grained correlation. Visualization results are compared in the supplementary material.

**Global vision feature and Multi-Query Estimator.** We remove both designs to validate the effectiveness of them. Specifically, by removing Multi-Query Estimator, the final results will be obtained by directly adding multiple masks, and by removing the global vision feature  $F_{vg}$ , we directly use the  $F_t$  in Eq.8 to generate queries. As shown in Table 4, removing either of them will achieve inferior performance than the default setting, and removing both of them get the worst result, demonstrating that both designs are vital for our method and their improvements can be complementary.

## 5 Conclusion

We introduce EAVL, an innovative framework for referring image segmentation, which leverages a novel Vision-Language Aligner to supplant convolutions with a fixed kernel in the segmentation stage. EAVL uses CLIP, harnessing its global and fine-grained information. By generating a series of queries and transforming them into query-based convolution kernels, the convolution kernels are directly related to the input language and image. Our approach explicitly aligns the vision and language, resulting in an effective text-to-pixel fine-grained correlation. Our experiments show that EAVL significantly outperforms previous state-of-the-art methods on RefCOCO, RefCOCO+ and G-Ref datasets. Extensive ablation studies validate the effectiveness of each proposed component.

Language: “a blond not facing us with suit on”



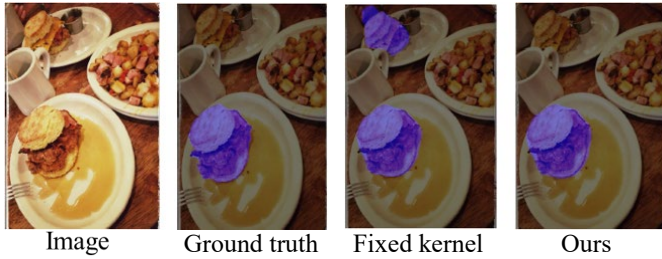
(a)

Language: “guy on the red bike”



(b)

Language: “sandwich by fork”



(c)

Language: “man in black”



(d)

Figure 4: Visualization of our method (using Vision-Language Aligner) and traditional method using convolutions with a fixed kernel in the segmentation stage.

## A Visualization

As shown in Figure 4, we provide visualization results of the ablation studies about the Vision-Language Aligner to demonstrate the effectiveness of this part in our proposed method. We take traditional methods using convolutions with a fixed kernel as the baseline. We visualize the results of our method and the baseline separately. From the visualization results, we can observe that the absence of the Vision-Language Aligner leads to worse segmentation masks. For instance, as illustrated in Figure 4(c), the language expression is “sandwich by fork,” but the baseline result displays two sandwiches. This is because the baseline method only notices the “sandwich” and does not fully correlate the “by fork” to the image in the pixel level. In our approach, we produce multiple queries, each with distinct emphases, such as queries highlighting “sandwich” and “by fork”. These queries are transformed into query-based kernels which are then employed for convolution in the segmentation stage, facilitating a comprehensive and explicit alignment between vision and language of varying emphases. As a result, our proposed method establishes a fine-grained correlation between text and pixels, effectively discerning distinctions between a sandwich with a fork and a sandwich without a fork at the pixel level. Similarly, as illustrated in Figure 4(a) and Figure 4(b), our method excels in achieving a more explicit alignment between language and image, resulting in better results, particularly in pixel-level details such as the left leg of the blond in Figure 4(a) and the left abdomen of the bike guy in Figure 4(b). These areas were previously disregarded by the baseline method. However, our model is still uncertain in some challenging marginal regions. As illustrated in Figure 4(d), the results of our method also included a small

part of another man’s hand. This instance shows there is still potential for improvement in our approach, particularly with regard to detailed areas.



## References

- Chen, L.-C.; Papandreou, G.; Kokkinos, I.; Murphy, K.; and Yuille, A. L. 2014. Semantic image segmentation with deep convolutional nets and fully connected crfs. *arXiv preprint arXiv:1412.7062*.
- Chen, Y.; Dai, X.; Liu, M.; Chen, D.; Yuan, L.; and Liu, Z. 2020. Dynamic convolution: Attention over convolution kernels. In *Proceedings of the IEEE/CVF conference on computer vision and pattern recognition*, 11030–11039.
- Deng, J.; Dong, W.; Socher, R.; Li, L.-J.; Li, K.; and Fei-Fei, L. 2009. Imagenet: A large-scale hierarchical image database. In *2009 IEEE conference on computer vision and pattern recognition*, 248–255. Ieee.
- Ding, H.; Liu, C.; Wang, S.; and Jiang, X. 2021. Vision-language transformer and query generation for referring segmentation. In *Proceedings of the IEEE/CVF International Conference on Computer Vision*, 16321–16330.
- Dosovitskiy, A.; Beyer, L.; Kolesnikov, A.; Weissenborn, D.; Zhai, X.; Unterthiner, T.; Dehghani, M.; Minderer, M.; Heigold, G.; Gelly, S.; et al. 2020. An image is worth 16x16 words: Transformers for image recognition at scale. *arXiv preprint arXiv:2010.11929*.
- Feng, G.; Hu, Z.; Zhang, L.; and Lu, H. 2021. Encoder fusion network with co-attention embedding for referring image segmentation. In *Proceedings of the IEEE/CVF Conference on Computer Vision and Pattern Recognition*, 15506–15515.
- He, K.; Zhang, X.; Ren, S.; and Sun, J. 2016. Deep residual learning for image recognition. In *Proceedings of the IEEE conference on computer vision and pattern recognition*, 770–778.
- Hu, R.; Rohrbach, M.; and Darrell, T. 2016. Segmentation from natural language expressions. In *Computer Vision–ECCV 2016: 14th European Conference, Amsterdam, The Netherlands, October 11–14, 2016, Proceedings, Part I 14*, 108–124. Springer.
- Jing, Y.; Kong, T.; Wang, W.; Wang, L.; Li, L.; and Tan, T. 2021. Locate then segment: A strong pipeline for referring image segmentation. In *Proceedings of the IEEE/CVF Conference on Computer Vision and Pattern Recognition*, 9858–9867.
- Kim, N.; Kim, D.; Lan, C.; Zeng, W.; and Kwak, S. 2022. Restr: Convolution-free referring image segmentation using transformers. In *Proceedings of the IEEE/CVF Conference on Computer Vision and Pattern Recognition*, 18145–18154.
- Krähenbühl, P.; and Koltun, V. 2011. Efficient inference in fully connected crfs with gaussian edge potentials. *Advances in neural information processing systems*, 24.
- Li, M.; and Sigal, L. 2021. Referring transformer: A one-step approach to multi-task visual grounding. *Advances in neural information processing systems*, 34: 19652–19664.
- Li, R.; Li, K.; Kuo, Y.-C.; Shu, M.; Qi, X.; Shen, X.; and Jia, J. 2018. Referring image segmentation via recurrent refinement networks. In *Proceedings of the IEEE Conference on Computer Vision and Pattern Recognition*, 5745–5753.
- Lin, T.-Y.; Maire, M.; Belongie, S.; Hays, J.; Perona, P.; Ramanan, D.; Dollár, P.; and Zitnick, C. L. 2014. Microsoft coco: Common objects in context. In *Computer Vision–ECCV 2014: 13th European Conference, Zurich, Switzerland, September 6–12, 2014, Proceedings, Part V 13*, 740–755. Springer.
- Liu, C.; Lin, Z.; Shen, X.; Yang, J.; Lu, X.; and Yuille, A. 2017. Recurrent multimodal interaction for referring image segmentation. In *Proceedings of the IEEE international conference on computer vision*, 1271–1280.
- Liu, Z.; Lin, Y.; Cao, Y.; Hu, H.; Wei, Y.; Zhang, Z.; Lin, S.; and Guo, B. 2021. Swin transformer: Hierarchical vision transformer using shifted windows. In *Proceedings of the IEEE/CVF international conference on computer vision*, 10012–10022.
- Luo, G.; Zhou, Y.; Ji, R.; Sun, X.; Su, J.; Lin, C.-W.; and Tian, Q. 2020a. Cascade grouped attention network for referring expression segmentation. In *Proceedings of the 28th ACM International Conference on Multimedia*, 1274–1282.
- Luo, G.; Zhou, Y.; Sun, X.; Cao, L.; Wu, C.; Deng, C.; and Ji, R. 2020b. Multi-task collaborative network for joint referring expression comprehension and segmentation. In *Proceedings of the IEEE/CVF Conference on computer vision and pattern recognition*, 10034–10043.
- Mao, J.; Huang, J.; Toshev, A.; Camburu, O.; Yuille, A. L.; and Murphy, K. 2016. Generation and comprehension of unambiguous object descriptions. In *Proceedings of the IEEE conference on computer vision and pattern recognition*, 11–20.
- Nagaraja, V. K.; Morariu, V. I.; and Davis, L. S. 2016. Modeling context between objects for referring expression understanding. In *Computer Vision–ECCV 2016: 14th European Conference, Amsterdam, The Netherlands, October 11–14, 2016, Proceedings, Part IV 14*, 792–807. Springer.
- Radford, A.; Kim, J. W.; Hallacy, C.; Ramesh, A.; Goh, G.; Agarwal, S.; Sastry, G.; Askell, A.; Mishkin, P.; Clark, J.; et al. 2021. Learning transferable visual models from natural language supervision. In *International conference on machine learning*, 8748–8763. PMLR.
- Wang, X.; Huang, Q.; Celikyilmaz, A.; Gao, J.; Shen, D.; Wang, Y.-F.; Wang, W. Y.; and Zhang, L. 2019. Reinforced cross-modal matching and self-supervised imitation learning for vision-language navigation. In *Proceedings of the IEEE/CVF conference on computer vision and pattern recognition*, 6629–6638.
- Wang, Z.; Lu, Y.; Li, Q.; Tao, X.; Guo, Y.; Gong, M.; and Liu, T. 2022. Cris: Clip-driven referring image segmentation. In *Proceedings of the IEEE/CVF conference on computer vision and pattern recognition*, 11686–11695.
- Yang, Z.; Wang, J.; Tang, Y.; Chen, K.; Zhao, H.; and Torr, P. H. 2022. Lavt: Language-aware vision transformer for referring image segmentation. In *Proceedings of the IEEE/CVF Conference on Computer Vision and Pattern Recognition*, 18155–18165.
- Yu, L.; Lin, Z.; Shen, X.; Yang, J.; Lu, X.; Bansal, M.; and Berg, T. L. 2018. Mattnet: Modular attention network for referring expression comprehension. In *Proceedings of the*

*IEEE conference on computer vision and pattern recognition*, 1307–1315.

Yu, L.; Poirson, P.; Yang, S.; Berg, A. C.; and Berg, T. L. 2016. Modeling context in referring expressions. In *Computer Vision–ECCV 2016: 14th European Conference, Amsterdam, The Netherlands, October 11–14, 2016, Proceedings, Part II 14*, 69–85. Springer.